Single Walled Carbon Nanohorns as Catalytic Counter Electrodes for Co(III)/(II) Electron Mediators in Dye Sensitized Cells

Stefano Carli,*[†] Laura Casarin,[†] Zois Syrgiannis,[‡] Rita Boaretto,[†] Elisabetta Benazzi,[†] Stefano Caramori,[†] Maurizio Prato[‡, §, ǁ] and Carlo Alberto Bignozzi[†]

[†]Department of Chemical and Pharmaceutical Sciences, University of Ferrara, Via Fossato di Mortara 17, 44121 Ferrara, Italy

[‡]Department of Chemical and Pharmaceutical Sciences, University of Trieste, Piazzale Europa 1, 34127 Trieste, Italy

[§]Carbon Nanobiotechnology Laboratory, CIC biomaGUNE, Paseo de Miramón 182, 20009 Donostia-San Sebastian, Spain

[ǁ] Basque Fdn Sci, Ikerbasque, Bilbao 48013, Spain

KEYWORDS: Single Walled Carbon Nanohorns, Dye Sensitized Solar Cells, Cobalt Redox Mediators, Electrochemical Impedance Spectroscopy, PEDOT.

ABSTRACT: The electrochemical properties of both pristine Single Walled Carbon Nanohorns (SWCNHS) and their chemically oxidized form (ox-SWCNHS) spray coated onto fluorine doped SnO_2 (FTO) were investigated in the framework of the fabrication of cobalt based transparent Dye Sensitized Solar Cells (DSSCs). These new nanocarbon substrates, evaluated in conjunction with the $Co(bpy)_3^{2+/3+}$ (bpy = 2,2' bipyridine) redox mediator, are endowed with excellent electrocatalytic properties, ease of fabrication and very promising stability and display a great potential for replacing the best noble metal and conductive polymer catalytic materials in the building of semi-transparent counter electrodes in new generation photoelectrochemical devices.

1. INTRODUCTION

In the framework of renewable energies, photoelectrochemical solar devices such as the Dye-sensitized solar cells (DSSCs), also known as "Grätzel cells, are currently subject of intense research, being low-cost photovoltaic devices which can be produced in transparent form with different colors and offer the possibility of integration in building facades. DSSC functioning is based on the cooperative interplay of subsystems such as the sensitized photoanode, the electron mediator and the catalytic counter electrode.[1]

Since the initial reports considerable effort has been directed towards the optimization of sensitizers,[2-4] redox mediators,[5-8] photoanode surface passivation[9,10] and counter electrodes.[11,12] The development of stable catalytic counter electrode materials characterized by high abundance, high electrochemical activity, tunable transparency and simple and scalable deposition routes is

relevant for the large scale applications of dye sensitized solar cells and of other emerging photoelectrochemical technologies.[13-15]

For the sake of low-cost, good stability, scalable deposition routes, morphological tunability, the p-type conducting polymer, poly(3,4-ethylenedioxythiophene) (PEDOT) has been successfully employed as organic counter electrode material, demonstrating promising electrocatalytic properties when investigated in conjunction with cobalt based redox mediators.[16-18]

Carbon based Nanomaterials have also been used to replace Pt counter electrodes.[19-25] Among them, Single Walled Carbon Nanohorns (**SWCNHS**) represents a very promising class of materials. [26] They are produced with a metal free synthesis and typically possess conical-shaped structures having diameter between 2 and 5 nm and length ranging around 80 nm (see **Figure 1**). These cones are associated in dahlia-type spherical structures with an average diameter of 100 nm.[27]

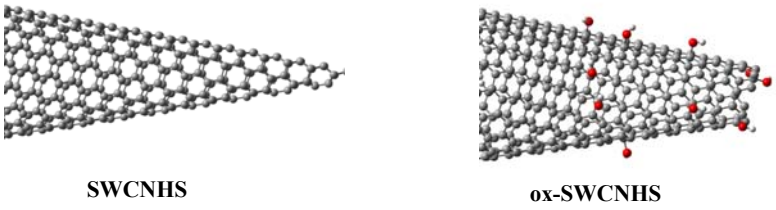

Figure 1. Typical 3D structure of pristine and oxidized Single Walled Carbon Nanohorns.

SWCNHS based materials have a number of characteristics which make them attractive for energy applications and photoelectrochemical cells.[26] They have large surface area (~400 $m^2 g^{-1}$ for the pristine materials), present semiconducting character and display magnetic properties.[28] In comparison with the other carbon nanomaterials **SWCNHS** are easier to disperse in organic solvents, allowing for their facile functionalization,[28] furthermore they can form porous films with high surface area.[29] **SWCNHS** have been recently implemented into ionic liquid based electrolytes[30] and used in composite materials mixed with cellulose and Pt clusters for the assembly of counter electrodes in iodide/triiodide based dye sensitized solar cells.[31] The surface area of **SWCNHS** can be tuned by chemical oxidation in acidic environments that promotes the opening of the horn tip preserving the conductivity and electrochemical properties (**Figure 1**).[32]

Herein we report, for the first time, the use of FTO-supported **SWCNHS** as catalytic counter electrodes in dye sensitized solar cells assembled with $Co(bpy)_3^{+2/+3}$ redox mediator (bpy = 2,2' bipyridine, Figure S1)[8]. Since it has been recently observed that carbon based nanomaterials tend to weakly adhere to FTO, leading to unstable devices,[8,19-21] oxidized Single Walled Carbon Nanohorns (**ox-SWCNHS**) were also employed. In fact, it has been described that chemical oxidation of carbon nanomaterials, using mineral acids such as HNO_3, produces a higher amount of carboxylic functional groups[33,34] that might be helpful to improve the adhesion to transparent conductive glass (FTO or ITO), thanks to a stronger interaction with the surface hydroxyl groups. Pedot has been selected as reference material for counter electrodes due to its well-established superior activity towards cobalt based redox mediators, thanks to the enhanced electroactive surface area and the reduced charge transfer resistance.[16] This work is devoted to both the evaluation of the electrocatalytic properties of these nanocarbon materials and to the

assessment of their electrocatalytic stability in association with cobalt based electrolytes in DSSCs.

2. EXPERIMENTAL SECTION

2.1 Materials and equipment.

Single Walled Carbon Nanohorns (**SWCNHs**) were produced by Carbonium s.r.l., Padova (Italy) by direct graphite evaporation in Ar flow, according to a patented method and used without purification.[35] Conductive FTO (fluorine tin oxide) TEC8, 2.3 mm thick substrates (Pilkington) were carefully cleaned by several washings in ethanol, acetone, and Alconox followed by annealing at 400 °C in air before use. TiO_2 colloidal paste (DSC 18NRT) was purchased from Dyesol. The organic dye LEG4 was from Dyenamo. Absorption spectra were collected with a JASCO V 570 UV–Vis spectrophotometer.

Thermogravimetric analyses (TGA) were performed using a TA Instruments TGA Q500 and recorded under N_2, upon equilibration at 100 °C, followed by a ramp of 10 °C/min up to 750 °C. Raman spectra were acquired with a Renishaw instrument, model Invia reflex equipped with 532, 633, and 785 nm lasers. After acquisition, the spectra were normalized with respect to the G band. Transmission electron microscopy (TEM) experiments were performed using a Philips EM 208, accelerating voltage of 100 kV. Samples were prepared by sonication for 10 min and dropwise addition (8 μL) of the sample onto a carbon coated 200 mesh Ni grid (EM Sciences,

Gibbstown, NJ) followed by solvent evaporation under vacuum. The surface morphology was investigated by Atomic force microscopy (AFM) measurements conducted with a Digital Instruments Nanoscope III Scanning Probe Microscope, Digital Instruments, CA, USA. The instrument was equipped with silicon tip (model RTESP-BRUKER resonant frequency 300 kHz) and operated in tapping mode. The scanning parameters were as follows: scan rate 1 Hz, resolution 512, and scan size 5 × 5 μm. Surface topographical analysis of raw AFM images was carried out with the NanoScope Analysis 1.5 program.

SEM imaging was performed with a Zeiss EVO 40 electronic microscope with a maximum acceleration voltage of 30 KV.

2.2 Typical procedure for the synthesis of ox-SWCNHS.

A 100 mg amount of pristine **SWCNHS** was dissolved in 100 ml HNO_3 4 M and the solution was stirred under reflux for 8 hours. The mixture was cooled to room temperature, 200 mL of water were added and the solution was filtered with Millipore apparatus. The material was repeatedly washed with water until the pH of the filtrate changed from acidic to neutral. The material was collected, re-dispersed in 200 mL of acetone with the aid of sonic bath irradiation for 10 minutes, filtered again with the Millipore apparatus and washed with 400 mL of acetone. The material was collected and dried under vacuum.

2.3 Procedure for the preparation of SWCNHS and ox-SWCNHS counter electrodes.

A suspension of the pristine **SWCNHS** or the oxidized **ox-SWCNHS** (1 mg ml^{-1}) in ethanol was sonicated for 30 minuts at room temperature. This suspension was sprayed over masked FTO electrodes (area 2×2.5 cm^2) placed on a hot plate at 120°C with an Air-brush (FENGDA 0.33mm) placed at distance of 15 cm from the plate, using N_2 as carrier (0.5 Pa). Electrodes were subsequently annealed at 400°C for 15 minutes.[31] The typical deposition procedure can be

summarized in table S1. The pristine **SWCNHS** (without any pretreatment) and the oxidized **ox-SWCNHS** were characterized by means of Thermogravimetric Analysis (TGA), Raman and IR spectroscopy.

2.4 Solar Cell and Symmetric Dummy Cell Fabrication. A compact TiO_2 blocking underlayer was prepared by spin-coating a 0,3 M titanium tetraisopropoxide solution in 1-butanol (1000 rpm for 10 s, 2000 rpm for 20 s). The resulting substrates were heated at 500 °C for 15 min and cooled to room temperature. Subsequently a mesoporous TiO_2 layer was prepared by doctor blading a commercial TiO_2 paste (Dyesol 18NR-T). The coated films were gradually heated to 500 °C according to the following programmed temperature ramping: rt - 120°C (10 min), 120°C - 450°C (30 min), 450°C (20 min), 450°C - 500°C (10 min), 500°C (10 min). After cooling to room temperature, the electrodes were treated with 0.4 M $TiCl_4$ overnight, washed with water and heated again at 450° for 30 minutes.

Solar cells and symmetrical cells were assembled by sealing the electrodes with 25 μm thick hot-melt film (Surlyn, Solaronix). The redox mediator was introduced thorough a small channel on the Surlyn frame. The active area was 0.20 cm^2 and 0.25 cm^2 for solar cells and symmetrical cells respectively. Finally the channel was sealed with epoxy resin. PEDOT based counter electrodes were prepared by potentiodynamic anodic electropolymerization of 3,4-ethylenedioxythiophene (EDOT) on FTO glasses, following our previously reported method.[36] Platinized FTO counter electrodes were prepared by screen-printing of a conductive colloidal platinum paste Chimet (Pt-10−004F-05, batch 5738) and were annealed at 400 °C for 10 min in air immediately before use.

2.5 Electrolyte Formulation. The electrolyte composition consisted of 0.18 M Co(II), 0.028 M Co(III) of $[Co(bpy)_3]^{2+/3+}$, 0.1 M $LiCF_3SO_3$ and 0.2 TBP in ACN for solar cell

characterization. The same electrolyte formulation in Methoxypropionitrile (MPN) was used for stability tests in dummy cells.

2.6 Solar Cell Characterization. Current−voltage measurements were performed with an Autolab PGSTAT 302/N potentiostat at a scan rate of 10 mV s^{-1}. Cell performances were evaluated under AM 1.5 illumination (ABET sun simulator).

2.7 Counter Electrode Characterization in Symmetric Cells.

Simmetric cells were investigated by slow scan rate cyclic voltammetry (SSCV) at 10 mV/s and by electrochemical impedance spectroscopy (EIS) by superimposing a sinusoidal 10 mV perturbation at the equilibrium potential (0 mV) of the assembled cell. Impedance data were analysed using commercially available Z-View software and were fitted in terms of equivalent electric circuits with relative errors < 5%.

3. RESULTS AND DISCUSSION

Among solution-processable deposition methods, such as spin coating, drop casting, dip coating etc., the spray coating technique, recently used to prepare graphene[37] based electrodes, was demonstrated to be a viable method for large-area fabrication of counter electrodes for DSSCs modules.

SWCNHS and **ox-SWCNHS** based counter electrodes have been prepared by spray coating the nanocarbon suspension (1 mg mL^{-1} in ethanol, see Section 2 for further details) onto cleaned FTO kept at 120°C on an hot plate: this technique was found to be the optimal solution in terms of homogeneity of deposition and reproducibility. The resulting electrodes were subsequently treated at 400° for 15 minutes to consolidate the coating. Carbon loading on the counter electrodes was evaluated through the measurement of the optical transmittance *T%* at a fixed

wavelength (550 nm) as previously reported.[19-21] Since the thickness of **SWCNHS** or **ox-SWCNHS** layers is a function of the number of cycles used during the spray coating deposition, for convenience we label **SWCNHS** or **ox-SWCNHS** according to their 550 nm transmission: for example **SWCNHS50** indicates a sample with $T\%_{550}$ = 50 %. PEDOT was chosen as the reference organic catalytic material due to its well demonstrated activity with respect to cobalt redox mediators.[16]

The amount of carboxyl groups created by oxidation of pristine **SWCNHS** with HNO_3 can be estimated by TGA. As shown in Figure 1, the weight loss at 300°C that has been reported to be related to CO_2 emission by the decomposition of carboxylic groups[38] is in the order of 1.7%, corresponding to a carbon losses of 0.46%. This means that the fraction of carbon atoms in the form of carboxylic functions in **ox-SWCNHS** is about 1% (0.4 mmol g^{-1}), [39] as confirmed also by acid-base titration.[40]

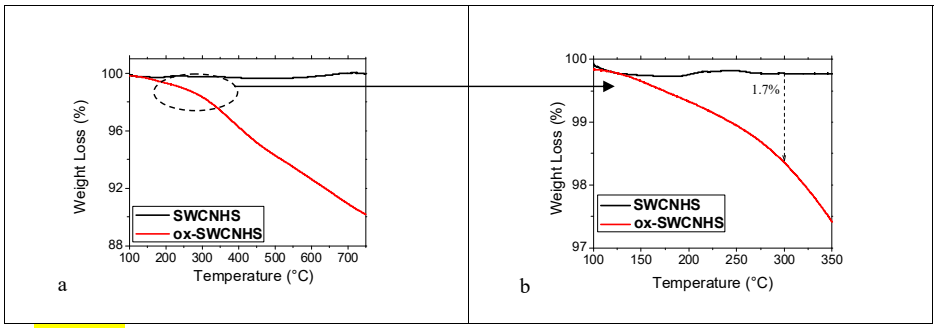

Figure 2. a) Thermogravimetric analysis of **SWCNHS** and **ox-SWCNHS** under N_2; b) magnification of the analysis plot in the temperature interval 100°C - 350°C.

These results are supported by Raman spectroscopy, where the covalent attachment of functionalizing groups on the **SWCNHS**, in the form of sp^3 carbon centers, can be detected from the normalized relative area ratio of the D-band with respect to the G-band (A_D/A_G) (Figure

3).[27,41-43] The normalized A_D/A_G ratio for the **ox-SWCNHS** is 1.22 with respect to the pristine material, showing a significant increase in the surface concentration of carboxylic groups in the sidewall of the **ox-SWCNHS** after the HNO_3 treated material.[44]

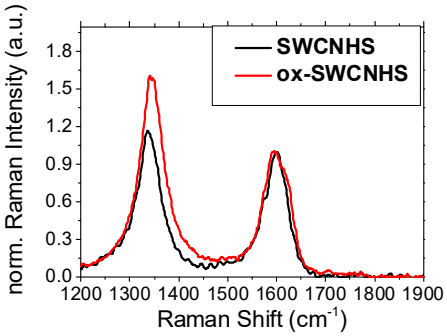

Figure 3. Raman spectra at 532 nm excitation wavelength of **SWCNHS** and **ox-SWCNHS** showing D (1350 cm^{-1}) and G bands (1600 cm^{-1}). [27]

The catalytic properties of the counter electrodes were investigated in thin layer (ca. 25 μm) dummy cells by slow scan rate cyclic voltammetry (SSCV) and by electrochemical impedance spectroscopy (EIS). SSCV leads to the evaluation of the limiting current J_L, expressed as $J_L = (2nFCD)/L$ (where L is the thickness of the spacer, C is the concentration of the redox couple, D is the diffusion coefficient) and of the differential resistance $(\partial\eta)/(\partial i)$ of the cell, calculated from the reciprocal slope of the linear trait of the i-V characteristic at low overpotentials. EIS provides deeper insights of the overall electrochemical process, by resolving charge transfer and mass transfer processes in the frequency domain. Impedance spectra, generally showing in the complex plain representation two depressed arcs (Figure 2b), were fitted with the electric equivalent reported in Figure S5 where R_S is the serial Ohmic resistance, R_{CT} is the charge

transfer resistance, CPE is the constant phase element and Z_W is the Nernst diffusion impedance of the thin layer cell.[45] While other authors added an additional pore diffusional impedance $Z_{W,\,pore}$ (Figure S2)[25] to describe the nature of a third high frequency semicircle observed at modified graphene/(I_3^-/I^-) interfaces, we did not observe such a feature and both a satisfactory fit and interpretation of EIS results was always achieved with the simplified model reported in Figure 4.

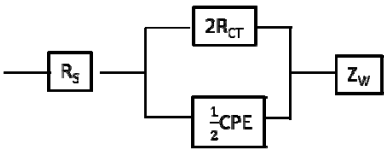

Figure 4. Reduced Electrical Equivalent Circuit of the Dummy Cell, used to fit EIS data.

An optimization of the spray deposition was performed in order to yield a good compromise between electrochemical response and optical transmissivity of the counter electrodes, required for building-integrated applications where transparency is an issue. In Figure 5 the SSCV (5a) and EIS plots (5b) of the dummy cells assembled with **SWCNHS5-20-60** counter electrodes, with their *T%* spectra (5c) are reported.

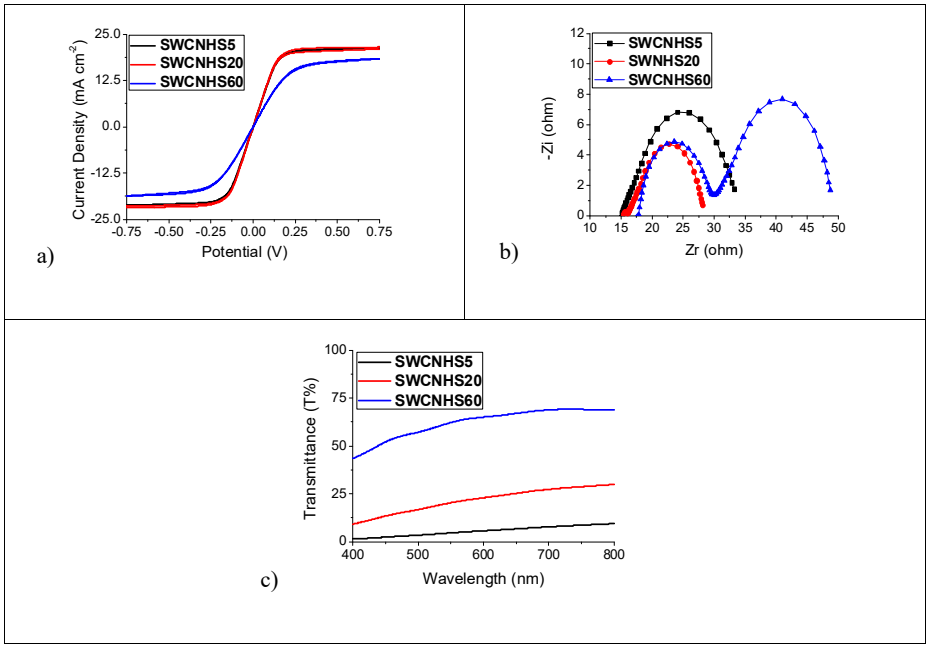

Figure 5. Thin layer cell characterization of **SWCNHS5-20-60** counter electrodes: a) SSCV recorder at 10 mV s^{-1} b) Nyquist plot recorded at 0 V, electrolyte composition 0.18 M Co(II), 0.028 M Co(III) of $[Co(bpy)_3]^{2+/3+}$, 0.1 M $LiCF_3SO_3$ and 0.2 TBP in ACN. c) *T%* spectra of CEs.

As can be seen in Figure 5a it is clear that the lowest limiting current and the highest overall resistance $(\partial\eta)/(\partial i)$ of the cell, are ascribed to **SWCNHS60,** consistent with EIS results at 0 V, showing, compared to **SWCNHS5** and **SWCNHS20,** larger charge transfer and diffusional arcs and lower film conductivity, evident from the high frequency intercept with the real axis. This indicates that, as expected, the tuning of the electroactive area, as a function of the SWCNH loading, is critical for optimizing the counter electrode response. Although the JV response of **SWCNHS20** and **SWCNHS5** was nearly superimposable, **SWCNHS20** was preferred to **SWCNHS5** since the former showed the lowest total impedance (Figure 5b) owing to the best compromise between transparency, conductivity, charge transfer and mass transfer resistance.

Similar results were obtained at comparable loading for the oxidized **ox-SWCNHS** (Figure S3). The electrocatalytic behavior of **SWCNHS20** and **ox-SWCNHS20** were compared with electrodeposited PEDOT[36], taken as reference organic catalytic material, (Figure 6 (a)-(c) and Table 1). **SWCNHS20**, **ox-SWCNHS20** and PEDOT exhibit JV curves having similar slope as well as limiting currents, ranging between 21 mA cm^{-2} for **ox-SWCNHS20** and 23 mA cm^{-2} for PEDOT, consistent with the resistive contributions extracted from the EIS analysis. It is interesting to observe that the SWCNH electrodes are generally better suited than PEDOT for transparent applications, providing comparable electrochemical response with a significantly superior transmittance, particularly in the NIR region (Figure 6c).

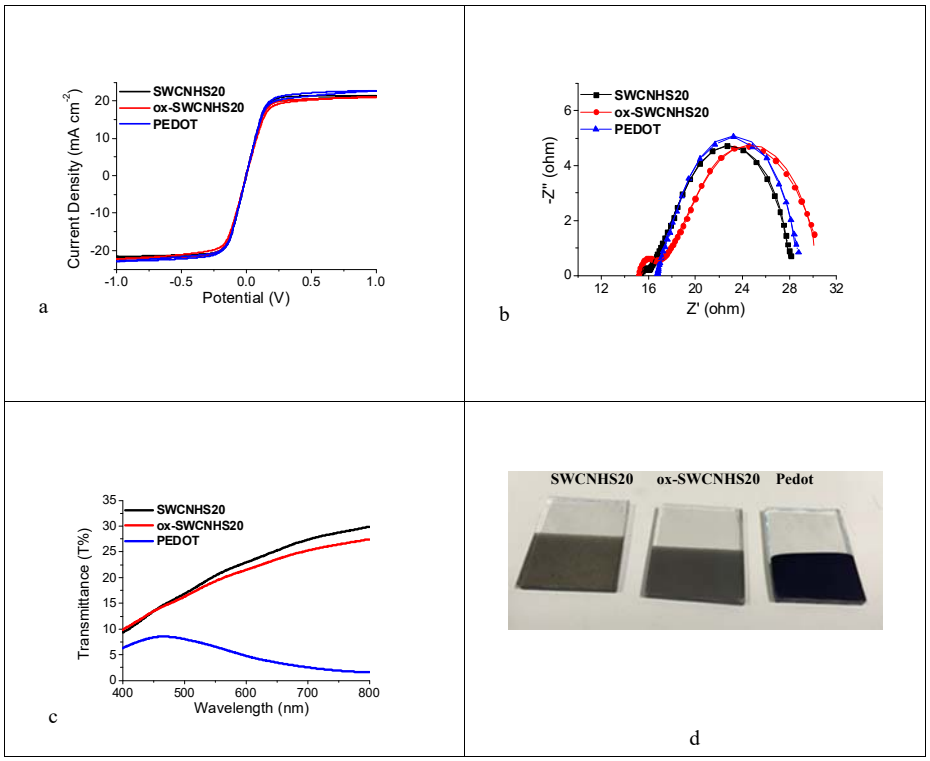

Figure 6. a) SSCV (10 mV s^{-1}) in thin layer cell: **SWCNHS20** (black), **ox-SWCNHS20** (red) and PEDOT (blue) b) Nyquist plots recorded at 0 V: **SWCNHS20** (black), **ox-SWCNHS20** (red) and PEDOT (blue), electrolyte composition 0.18 M Co(II), 0.028 M Co(III) of $[Co(bpy)_3]^{2+/3+}$, 0.1 M $LiCF_3SO_3$ and 0.2 TBP in ACN; c) *T%* spectra of CEs and d) counter electrodes picture.

Transparent platinum coated dummy cells filled with the cobalt based electrolyte in ACN exhibit a certain variability in their electrochemical response, consistent with other reports about the electrochemical behavior of cobalt polypyridine couples at noble metal electrodes. [Ashbrook, L.N.; Eliott, C.M., J.Phys.Chem.C 2014, 118, 16643-16650]. In general the charge transfer resistance of platinum electrode is higher than those found for NHs and PEDOT, and this effect could be exacerbated by adsorption of electrolyte components like Tert-butyl-Pyridine on the noble metal surface, resulting in rapid (with respect to time) decrease of the heterogeneous charge transfer kinetics. Indeed electrochemical stability tests in sealed dummy cells containing Co(III)/(III) in MPN reveal, during the arc of few days, a significant decrease of the slope of the i-V characteristics paralleled by a drop in limiting current (Figure SXX). This effect is consistent with an increased charge transfer resistance, revealed by impedance spectroscopy Figure S.XX.

Formattato: Evidenziato

Formattato: Colore carattere: Rosso, Evidenziato

Formattato: Evidenziato

Eliminato: T

Eliminato: is

Eliminato: partly due to

Eliminato: fast

Eliminato: in

Eliminato: n

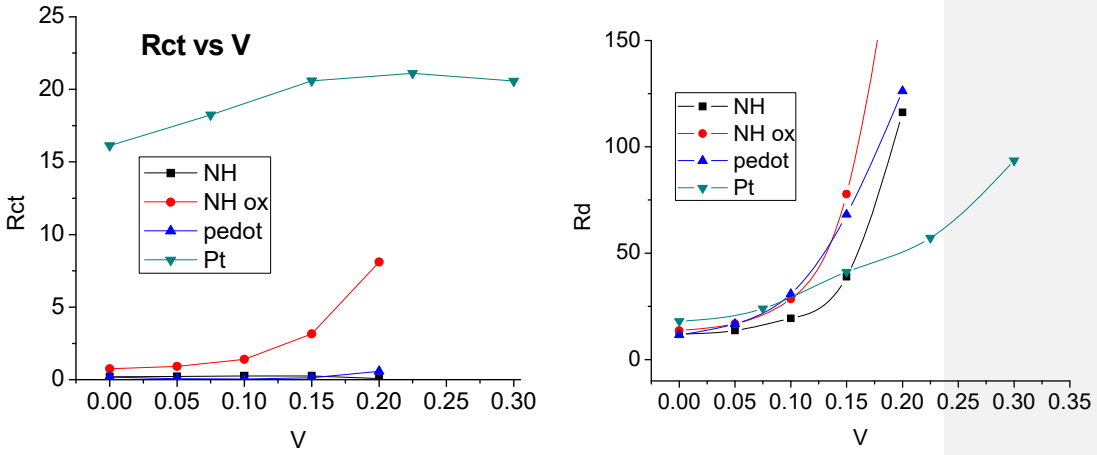

Figure 7. Charge transfer (A) and diffusional resistance (B) extracted from fits of impedance data in symmetric thin layer cells. Please note the difference in the scales of Rd and Rct showing that diffusion is the major component of the cell resistance. The charge transfer resistance is essentially constant, while the diffusonal resistance undergoes a fast increase as the limiting current is approached. The apparent increase in the Rct of NHox is probably an artifact caused the by the difficult deconvolution of the small Rct from the very large Rd.

Formattato: Tipo di carattere: Non Grassetto, Evidenziato

Formattato: Tipo di carattere: Non Grassetto, Evidenziato

Formattato: Tipo di carattere: Non Grassetto

Table 1. Relevant Parameters Extracted from the EIS Study in Dummy Cells (0.25 cm^2 Active Area) at 0 V.

	J_L (mA cm^{-2})	Slope (mA V^{-1})	$(slope)^{-1}$ (Ω)	R_s (Ω)	R_{CT} (Ω)	R_D (Ω)	R_{tot} (Ω)
SWCNHS20	21.4	35.6	28.1	15.5	0.21	12.0	27.9
ox-SWCNHS20	21.0	32.2	31.0	15.2	0.75	13.6	30.3
PEDOT	22.7	35.8	27.9	16.7	0.18	11.5	28.7

While **SWCNHS20** and **PEDOT** exhibit very similar R_{CT} and R_D, of the order of 0.2 Ω and 12 Ω respectively it can be observed that **ox-SWCNHS20** is characterized by higher R_{CT} and R_D. The surface morphology of the electroactive material is usually the determinant factor in explaining such differences. Scanning electron microscopy (SEM), atomic force microscopy

(AFM) and Transmission Electron Microscopy (TEM) analysis have been used to explore the morphological properties of the two different types of carbon nanohorn based substrates. SEM imaging (Figure 7) shows that **SWCNHS20** exhibits a very homogeneous and porous "sponge-like" surface with cavities of the order of 100-250 nm, whereas the morphology of **ox-SWCNHS20** is clearly less porous, presenting larger aggregates with diameters up to ca 1μm, irregularly distributed on the surface.

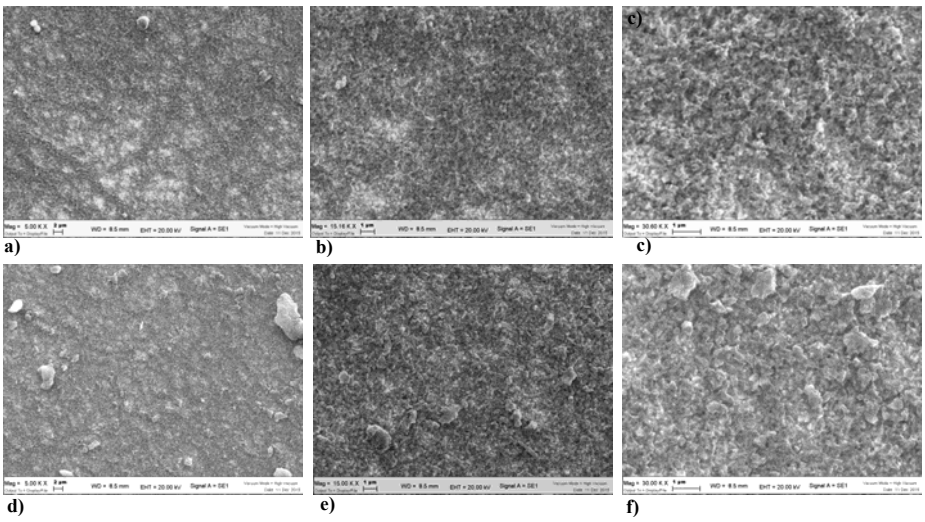

Figure 7. SEM micrograph of (a), (b), (c) **SWCNHS20** and of (d), (e), (f) **ox-SWCNHS20**.

AFM analysis (Figure 8 and Table 2) substantially corroborated the qualitative observations carried out by SEM, showing a slightly higher surface roughness in **ox-SWCNHS20** compared to **SWCNHS20** (Rq = 101 nm Vs 77 nm for **SWCNHS20**) indicating a less regular surface coverage. This is particularly evident in the 3D AFM view: the higher R_{max} (i.e. the average vertical distance between the deepest valley and highest peak) observed for **ox-SWCNHS20**, is indeed affected by the presence of big carbon lumps irregularly distributed on the surface. This observation is consistent with TEM imaging showing, in **ox-SWCNHS20,** the formation of spherical aggregates with diameter in the order of 500 nm. On the contrary, pristine **SWCNHS20** preserve a more homogeneous distribution with smaller interconnected aggregates (ca. 100 nm) exhibiting a higher content of tips on the borders, contributing to enhance the electroactive area of the catalyst (Figure 8).

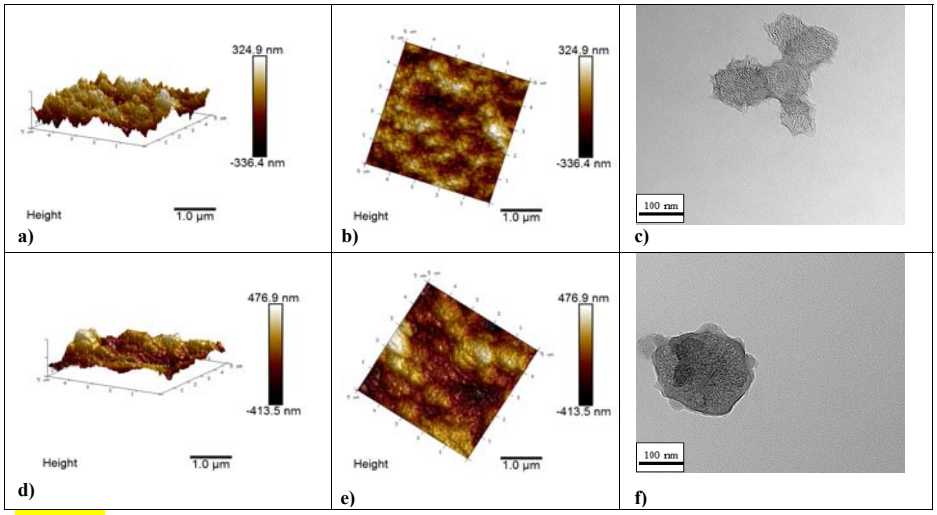

Figure 8. AFM imaging of (a), (b) **SWCNH20** and (d), (e) **ox-SWCNH20**. TEM micrograph of (c) **SWCNH20** and (f) **SWCNH20**.

Table 2. Surface Morphology Parameters for **SWCNHS20** and **ox-SWCNHS20** films obtained from AFM Analysis.[a]

CEs	R_q (nm)	R_a (nm)	R_{max} (nm)
SWCNHS20	96.1	77.4	693
ox-SWCNHS20	127	101	810

R_q: Root mean square: average of height deviations taken from the mean image data plane; R_a: Arithmetic average of the absolute values of the surface height deviations measured from the mean plane; R_{max}: Maximum vertical distance between the highest and lowest data points in the image following the planefit.

The stability of **SWCNHS20**, **ox-SWCNHS20** and PEDOT based counter electrodes has been evaluated in sealed dummy cells based on the $Co(bpy)_3^{+2/+3}$ redox mediator in methoxypropionitrile (MPN) having a better long term stability with respect to acetonitrile, commonly used in record cells (Figure 9 and S5).[46] The higher viscosity of MPN explains the lower limiting current (10-15 mA cm^2) observed with the nanohorn modified electrodes. The assembled cells were monitored by both SSCV and EIS at room temperature, finding a progressive increase in the electrochemical performance of the nanocarbon coated electrodes during the first 10 days, until attaining a stable response which is then stably maintained. The EIS analysis show a progressive decrease of the resistance associated to the diffusional arc, which is consistent with a progressive and more intimate permeation of the carbon film by the redox mediator, leading to the consequent enhancement in limiting current. Similar results were observed for graphene based counter electrodes during ageing tests.[21] By contrast, although freshly prepared PEDOT films show excellent performance, a progressive decay of their electrochemical response is observed over the first 10 days, both due to an increase of the diffusional resistance and of the series ohmic resistance, which can be appreciated from the shift of the high frequency intercept of the arc on the real axis. These results could be motivated by a loss of adhesion of the conducting polymer from the underlying FTO contact and by adsorption

of the redox mediator or of other electrolyte additives at the polymer surface, constituting local blocking layers for both the electron transfer and mass transfer. The increase of the PEDOT interfacial charge transfer resistance from ca. 7 Ω in the freshly sealed cell to ca. 12 Ω also corroborates this latter effect.

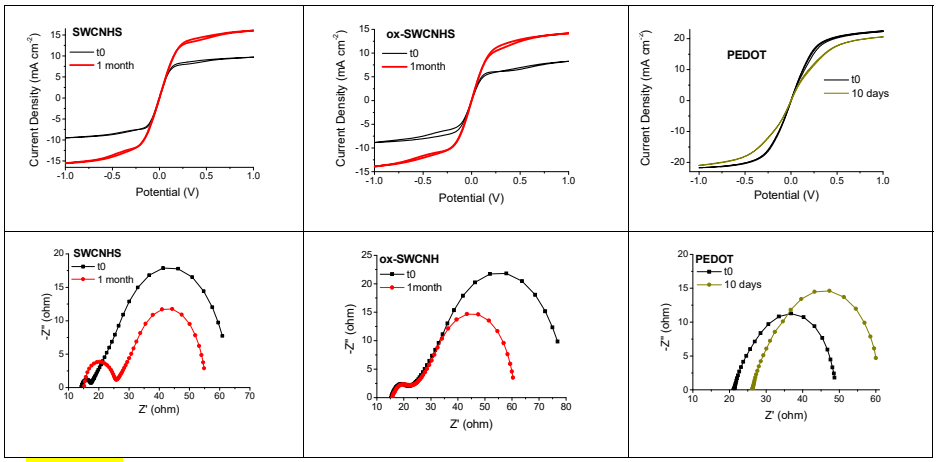

Figure 9. Long term electrochemical response evaluated in sealed dummy cell at room temperature: cells were first cycled to attain a steady electrochemical response (superimposable curves), and subsequently analyzed by EIS at 0V after 10 s relaxation (at 0 V). Electrolyte composition 0.18 M Co(II), 0.028 M Co(III) of $[Co(bpy)_3]^{2+/3+}$, 0.1 M $LiCF_3SO_3$ and 0.2 TBP in MPN.

The nanohorn counter electrodes have been tested in solar devices assembled with the carbazole based organic dye LEG4 (Figure S6) whose sterically hindered structure efficiently blocks recombination involving conduction band electrons and $Co(bpy)_3^{3+}$.[3] Consistent with the

dummy cell results, the nanohorns electrodes exhibit comparable efficiency with PEDOT based CEs ($\eta > 6.7$ % in all cases) (Figure 10 and Table 3), however, they offer the additional benefits of a higher reproducibility in performances (Figure S7) and can be prepared through spray coating, which represents the ideal method for the fabrication of large-area DSSCs. Among the counter electrode materials selected for this study, the use of platinum results in the lowest performances, ascribable to the highest charge transfer resistance, as discussed before.

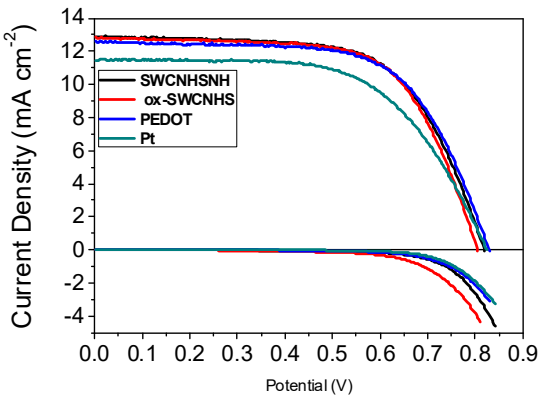

Figure 10. Current-voltage characteristics of DSSC with LEG4 sensitized TiO_2 photoanodes under AM 1.5G. Electrolyte composition: $Co(bpy)_3^{+2/+3}$ 0.18M/0.028M, $LiCF_3SO_3$ 0.1M, TBP 0.2M in ACN.

Table 3. Efficiency parameters obtained from the JV curves reported in Figure 6.

CEs	J_{sc} (mA cm^{-2})	V_{oc} (V)	FF	η %
SWCNH	12.91	0.82	0.64	**6.76**
ox-SWCNH	12.84	0.80	0.66	**6.75**
PEDOT	12.58	0.83	0.64	**6.73**
Pt	11.46	0.82	0.61	**5.74**

4 CONCLUSIONS

In summary, counter electrodes built by spraying Single Walled Carbon Nanohorns on FTO electrodes were prepared and their electrocatalytic properties were for the first time investigated in conjunction with the $Co(bpy)_3^{+2/+3}$ redox mediator. These new substrates coupling excellent electrocatalytic properties, ease of fabrication and very promising stability might constitute a viable replacement to noble metal and conductive polymer based materials for building counter electrodes for new generation photoelectrochemical devices.

ASSOCIATED CONTENT

Supporting Information. Chemical formula of the cobalt based redox mediator and of the LEG4 dye, as well as the alternative reduced electrical equivalent circuit, the JV statistics on the DSSCs, and electrochemical stability tests on different types of (semi) transparent counter electrodes, are available free of charge *via* the Internet at http://pubs.acs.org.

Eliminato: D

Eliminato: and additional information

AUTHOR INFORMATION

Corresponding Author

E-mail: crlsfn@unife.it

Author Contributions

The manuscript has been written with the contribution of all authors. All authors have given approval to the final version of the manuscript.

Funding Sources

Financial support from the Italian Ministero dell'Università e della Ricerca (MIUR), (FIRB RBAP11C58Y, "NanoSolar", PRIN 2010 "Hi-Phuture" and PRIN 2010 "DSSCX" are gratefully acknowledged

REFERENCES

1. O'Regan, B.; Grätzel, M. A Low-cost, High-Efficiency Solar Cell Based on Dye Sensitized Colloidal TiO_2 Films *Nature* **1991**, *353*, 737-740.

2. Urbani, M.; Grätzel, M.; Nazeeruddin, M. K.; Torres, T. Meso-Substituted Porphyrins for Dye-Sensitized Solar Cells *Chem. Rev*. **2014**, *114*, 12330−12396.

3. Gabrielsson, E.; Ellis, H.; Feldt , S.; Tian, H.; Boschloo, G.; Hagfeldt, A.; Sun, L. Convergent/Divergent Synthesis of a Linker-Varied Series of Dyes for Dye-Sensitized Solar Cells Based on the D35 Donor *Adv. Energy Mater*. **2013**, *3*, 1647–1656.

4. Tsao , H. N.; Yi , C.; Moehl, T.; Yum, J. H.; Zakeeruddin, S. M.; Nazeeruddin, M. K.; Grätzel, M. Cyclopentadithiophene Bridged Donor–Acceptor Dyes Achieve High Power Conversion Efficiencies in Dye-Sensitized Solar Cells Based on the tris-Cobalt Bipyridine Redox Couple *ChemSusChem* **2011**, *4*, 591 - 594.

5. Wu, J.; Lan, Z.; Lin, J.; Huang, M.; Huang, Y.; Fan, L.; Luo, G. Electrolytes in Dye-Sensitized Solar Cells *Chem. Rev.* **2015**, *115*, 2136−2173.

6. Bella, F.; Vlachopoulos, N.; Nonomura, K.; Zakeeruddin, S. M.; Grätzel, M.; Gerbaldia, C.; Hagfeldt, A. Direct Light-induced Polymerization of Cobalt-Based Redox Shuttles: An

Ultrafast Way Towards Stable Dye-Sensitized Solar Sells *Chem. Commun.* **2015**, *51*, 16308-16311.

7. Carli, S.; Benazzi, E.; Casarin, L.; Bernardi, T.; Bertolasi, V.; Argazzi, R.; Caramori, S.; Bignozzi, C. A. On The Stability of Manganese tris(β-diketonate) Complexes as Redox Mediators in DSSCs *Phys. Chem. Chem. Phys.* **2016**, *18*, 5949-5956.

8. Sapp, S. A.; Elliot, M.; Contado, C.; Caramori, S.; Bignozzi, C. A. Substituted Polypyridine Complexes of Cobalt(II/III) as Efficient Electron-Transfer Mediators in Dye-Sensitized Solar Cells *J. Am. Chem. Soc.* **2002**, *124*, 11215−11222.

9. Carli, S.; Casarin, L.; Caramori, S.; Boaretto, R.; Busatto, E.; Argazzi, R.; Bignozzi, C. A. A Viable Surface Passivation Approach To Improve Efficiency in Cobalt Based Dye Sensitized Solar Cells *Polyhedron* **2014**, *82*, 173-180.

10. Kakiage, K.; Aoyama, Y.; Yano, T.; Oya, K.; Fujisawa, J. I.; Hanay, M. Highly-Efficient Dye-Sensitized Solar Cells With Collaborative Sensitization by Silyl-anchor and Carboxy-anchor Dyes *Chem. Commun.* **2015**, *51*, 15894-15897.

11. Wu, M.; Ma, T. Recent Progress of Counter Electrode Catalysts in Dye-Sensitized Solar Cells *J. Phys. Chem. C* **2014**, *118*, 16727−16742.

12. Yun, S.; Hagfeldt , A.; Ma, T. Pt-Free Counter Electrode for Dye-Sensitized Solar Cells with High Efficiency *Adv. Mater.* **2014**, *26*, 6210-6237.

13. Li, Z.; Kulkarni, S. A.; Boix, P. P.; Shi, E.; Cao, A.; Fu, K.; Batabyal, S. K.; Zhang, J.; Xiong, Q.; Wong, L. H.; Mathews, N.; Mhaisalkar, S. G. Laminated Carbon Nanotube Networks for Metal Electrode-Free Efficient Perovskite Solar Cells *ACS Nano* **2014**, *8*, 6797-6804.

14. Zhang, F.; Yang, X.; Wang, H.; Cheng, M.; Zhao, J.; Sun, L. Structure Engineering of Hole–Conductor Free Perovskite-Based Solar Cells with Low-Temperature-Processed Commercial Carbon Paste As Cathode *ACS Appl. Mater. Interfaces* **2014**, *6*, 16140-16146.

15. Zhang, F.; Yanga, X.; Cheng, M.; Wang, W.; Sun, L. Boosting The Efficiency and The Stability of Low Cost Perovskite Solar Cells by Using CuPc Nanorods as Hole Transport Material and Carbon as Counter Electrode *Nano Energy* **2016**, *20*, 108-116.

16. Carli, S.; Busatto, E.; Caramori, S.; Boaretto, R.; Argazzi, R.; Timpson, C. J.; Bignozzi, C. A. Comparative Evaluation of Catalytic Counter Electrodes for Co(III)/(II) Electron Shuttles in Regenerative Photoelectrochemical Cells *J. Phys. Chem. C* **2013**, *117*, 5142−5153.

17. Park, B. W.; Pazoki, M.; Aitola, K.; Jeong, S.; Johansson, E. M. J.; Hagfeldt, A.; Boschloo, G. Understanding Interfacial Charge Transfer between Metallic PEDOT Counter Electrodes and a Cobalt Redox Shuttle in Dye-Sensitized Solar Cells *ACS Appl. Mater. Interfaces* **2014**, *6*, 2074−2079.

18. Ellis, H.; Vlachopoulos, N.; Häggman, L.; Perruchot, C.; Jouini, M.; Boschloo, G.; Hagfeldt, A. EDOT Counter Electrodes for Dye-Sensitized Solar Cells Prepared by Aqueous Micellar Electrodeposition *Electrochim. Acta* **2013**, *107*, 45-51.

19. Kavan, L.; Yum, J. H.; Nazeeruddin, M. K.; Grätzel, M. Graphene Nanoplatelet Cathode for Co(III/II) Mediated Dye-Sensitized Solar Cells *ACS Nano* **2011**, *5*, 9171−9178.

20. Kavan, L.; Yum, J. H.; Grätzel, M. Optically Transparent Cathode for Dye-Sensitized Solar Cells Based on Graphene Nanoplatelets *ACS Nano* **2011**, *5*, 165−172.

21. Kavan, L.; Yum, J. H.; Grätzel, M. Graphene Nanoplatelets Outperforming Platinum as the Electrocatalyst in Co-Bipyridine-Mediated Dye-Sensitized Solar Cells *Nano Lett.* **2011**, *11*, 5501-5506.

22. Poudel, P.; Qiao, Q. Carbon Nanostructure Counter Electrodes For Low Cost and Stable Dye-Sensitized Solar Cells *Nano Energy* **2014**, *4*, 157-175.

23. Kavan, L.; Yum, J. H.; Grätzel, M. Optically Transparent Cathode for Co(III/II) Mediated Dye-Sensitized Solar Cells Based on Graphene Oxide *ACS Appl. Mater. Interfaces* **2012**, *4*, 6999–7006.

24. Roy-Mayhew, J. D.; Boschloo, G.; Hagfeldt, A.; Aksay, I. A. Functionalized Graphene Sheets as a Versatile Replacement for Platinum in Dye-Sensitized Solar Cells *ACS Appl. Mater. Interfaces* **2012**, *4*, 2794−2800.

25. Roy-Mayhew, J. D.; Bozym, D. J.; Punckt, C.; Aksay, I. A. Functionalized Graphene as a Catalytic Counter Electrode in Dye-Sensitized Solar Cells *ACS Nano* **2010**, *4*, 6203−6211.

26. Z. Zhang; S. Han; C. Wang; J. Li; G. Xu. Single-Walled Carbon Nanohorns for Energy Applications *Nanomaterials* **2015**, *5*, 1732.

27. Yudasaka, M.; Iijima, S.; Crespi, V. H., Single-Wall Carbon Nanohorns and Nanocones *Top. Appl. Phys.* **2008**, *111*, 605-629.

28. Zhu, S.; Xu, G. Single-Walled Carbon Nanohorns and their Applications *Nanoscale* **2010**, *2*, 2538-2549.

29. Urita, K.; Seki, S.; Utsumi, S.; Noguchi, D.; Kanoh, H.; Tanaka, H.; Hattori, Y.; Ochiai, Y.; Aoki, N.; Yudasaka, M.; Iijima, S.; Kaneko, K. Effects of Gas Adsorption on the Electrical Conductivity of Single-Wall Carbon Nanohorns *Nano Lett.* **2006**, *6*, 1325-1328.

30. Lodermeyer, F.; Costa, R. D.; Casillas, R.; Kohler, F. T. U.; Wasserscheid, P.; Prato, M.; Guldi, D. M. Carbon Nanohorn-Based Electrolyte for Dye Sensitized Solar Cells *Energy Environ. Sci.* **2015**, *8*, 241-246.

31. Cruz, R.; Brandão, L.; Mendes, A. Use of Single-Wall Carbon Nanohorns as Counter Electrodes in Dye-Sensitized Solar Cells *Int. J. Energy Res.* **2013**, *37*, 1498-1508.

32. Brandão, L.; Boaventura, M.; Passeira, C.; Gattia, D. M.; Marazzi, R.; Antisari, M. V.; Mendes, A. An Electrochemical Impedance Spectroscopy Study of Polymer Electrolyte Membrane Fuel Cells Electrocatalyst Single Wall Carbon Nanohorns-Supported *J. Nanosci. Nanotechnol.* **2011**, *11*, 9016-9024.

33. Wepasnick, K. A.; Smith, B. A.; Schrote , K. E.; Wilson , H. K.; Diegelmann, S. R.; Fairbrother, D. H. Surface and Structural Characterization of Multi-Walled Carbon Nanotubes Following Different Oxidative Treatments *Carbon* **2011**, *49*, 24-36.

34. Jung, J.; Graupner, R.; Ley, L.; Hirsch, A. Quantitative Determination of Oxidative Defects on Single Walled Carbon Nanotubes *Phys. Status Solidi B* **2006**, *243*, 3217–3220.

35. Schiavon, M. Device and method for production of carbon nanotubes, fullerene and their derivatives *EP1428794 (A2)*, **2006**.

36. Carli, S.; Casarin, L.; Bergamini, G.; Caramori, S.; Bignozzi, C. A. Conductive PEDOT Covalently Bound to Transparent FTO Electrodes *J. Phys. Chem. C* **2014**, *118*, 16782-16790.

37. Casaluci, S.; Gemmi, M.; Pellegrini, V.; Di Carlo, A.; Bonaccorso, F. Graphene-Based Large Area Dye-Sensitized Solar Cell Module *Nanoscale* **2016**, *8*, 5368-5378.

38. Figueiredo, J. L.; Pereira, M. F. R.; Freitas, M. M. A.; Òrfão, J. J. M. Modification of the Surface Chemistry of Activated Carbons *Carbon* **1999**, *37*, 1379-1389.

39. Nakamura, M.; Irie, M.; Yuge, R.; Ichihashi, T.; Iijima, S.; Yudasaka, M. Carboxylation of Thin Graphitic Sheets Is Faster than that of Carbon Nanohorns *Phys. Chem. Chem. Phys.* **2013**, *15*, 16672-16675.

40. Eschemann, T. O.; Lamme, W. S.; Manchester, R. L.; Parmentier, T. E.; Cognigni, A.; Rønning, M.; de Jong, K. P. Effect of Support Surface Treatment on the Synthesis, Structure, and Performance of Co/CNT Fischer–Tropsch Catalysts *J. Catal.* **2015**, *328*, 130-138.

41. Rotas, G.; Sandanayaka, A. S. D.; Tagmatarchis, N.; Ichihashi, T.; Yudasaka, M.; Iijima, S.; Ito, O. (Terpyridine)copper(II)−Carbon Nanohorns: Metallo-nanocomplexes for Photoinduced Charge Separation *J. Am. Chem. Soc.* **2008**, *130*, 4725-4731.

42. Sandanayaka, A. S. D.; Pagona, G.; Fan, J.; Tagmatarchis, N.; Yudasaka, M.; Iijima, S.; Araki, Y.; Ito, O. Photoinduced Electron-Transfer Processes of Carbon Nanohorns with

Covalently Linked Pyrene Chromophores: Charge-Separation and Electron-Migration Systems *J. Mater. Chem.* **2007**, *17*, 2540-2546.

43. Cioffi, C.; Campidelli, S.; Sooambar, C.; Marcaccio, M.; Marcolongo, G.; Meneghetti, M.; Paolucci, D.; Paolucci, F.; Ehli, C.; Rahman, G. M. A.; Sgobba, V.; Guldi, D. M.; Prato, M. Synthesis, Characterization, and Photoinduced Electron Transfer in Functionalized Single Wall Carbon Nanohorns *J. Am. Chem. Soc.* **2007**, *129*, 3938-3945.

44. Yuge, R.; Bandow, S.; Nakahara, K.; Yudasaka, M.; Toyama, K.; Yamaguchi, T.; Iijima, S.; Manako, T. Structure and Electronic States of Single-Wall Carbon Nanohorns Prepared Under Nitrogen Atmosphere *Carbon* **2014**, *75*, 322-326.

45. Hauch, A.; Georg, A. Diffusion in the Electrolyte and Charge-Transfer Reaction at the Platinum Electrode in Dye-Sensitized Solar Cells *Electrochim. Acta* **2001**, *46*, 3457-3466.

46. Hagfeldt, A.; Boschloo, G.; Sun, L.; Kloo, L.; Pettersson, H. Dye-Sensitized Solar Cells *Chem. Rev.* **2010**, *110*, 6595-6663.

TOC